Received 26 December 2023; accepted 10 January 2024. Date of publication 16 January 2024; date of current version 26 March 2024.

Digital Object Identifier 10.1109/OJAP.2024.3354818

Compact Dielectric Resonator Antenna With Improved Bandwidth via Loading of Metal Ring

HUI GU [1,2] AND LEI GE [2] (Senior Member, IEEE)

[1]School of Electronics and Information, Hangzhou Dianzi University, Hangzhou 310018, China

[2]State Key Laboratory of Radio Frequency Heterogeneous Integration, Shenzhen University, Shenzhen 518000, China

CORRESPONDING AUTHOR: L. GE (e-mail: leige@szu.edu.cn)

This work was supported in part by the National Natural Science Foundation of China under Grant 62071308, and in part by the Shenzhen Science and Technology Program under Grant ZDSYS20220527171402005.

ABSTRACT In this paper, a novel dielectric resonator antenna (DRA) characterized by a compact size and wide bandwidth is proposed. The achievement of wideband performance involves the introduction of a metallic ring structure inside the dielectric resonato, ensuring that the antenna's volume remains compact. Fundamental and higher-order modes, $TM_{01\delta}$, $TM_{021+\delta}$ of the cylinder DRA are first investigated by using E-field distribution analysis, and it is found that these two modes are hard to resonate in proximity to each other. Therefore, a thin metal ring, acting as a perturbation structure is inserted into the DR to perturb the E-field of the higher-order mode and reduce its resonant frequency. Consequently, the resonant frequency of the $TM_{021+\delta}$ mode is significantly decreased, with only a slight effect on the $TM_{01\delta}$ mode. The resonant frequencies of the three resonances, i.e., $TM_{01\delta}$, $TM_{021+\delta}$ and probe-mode, are moved in proximity to achieve a wide impedance bandwidth. For experimental validation, a prototype is fabricated and tested. The measured results show the proposed antenna achieves a bandwidth of 51.1% with a low profile of $0.156\lambda_c$, where λ_c represents the wavelength at the center frequency. With these advantages, the proposed design is well-suited for mounting on vehicle platforms, particularly for 4G (2.6 GHz) and 5G (3.5 GHz) communications.

INDEX TERMS Dielectric resonator antenna (DRA), bandwidth improvement, vehicular communications.

I. INTRODUCTION

DIELECTRIC resonator antennas (DRAs) have been studied extensively over the past years since they were reported by Long et al. in 1983 [1]. With the advantages of compact size, light weight, low cost and more degrees of freedom than 1-D-type and 2-D-type antennas [2], [3], [4], they have become a promising candidate for many wireless communication systems, such as vehicular communications and mobile communications. In vehicular communications, except for a wide band to cover more wireless frequencies, low profile and small footprint are also highly desired. By employing compact wideband antennas, systems can achieve high data rates and throughout in complex vehicular networks [5], [6], [7].

Seceral bandwidth enhancement techniques have been developed for the design of DRAs. One straightforward method involves using stacked structures or introducing parasitic dielectric elements around the feeding probe. In [8], [9], an impedance bandwidth of more than 35% was achieved by vertically stacking two different DRs. To further broaden the bandwidth, various designs, such as multi-segment DRA [10], T-shaped DRA [11], or multi-layered DRA [12], have been developed. These designs can achieve a 10-dB impedance bandwidth of higher than 60%. The introduction of parasitic elements has been shown to increase bandwidth, as demonstrated in [13]. However, these reported designs tend to increase the complexity or profile of DRAs, even with the enhanced bandwidth. Low-profile DRAs with a height of approximately $0.1\lambda_0$ (where λ_0 is the free-space wavelength) was exploited in [14], [15], [16]. Nonetheless, the achieved bandwidth in these cases was relatively narrow.

The impedance bandwidth of DRAs can be enhanced through the use of modified shapes, as explored in [17], [18], [19], [20]. In [17], an inverted truncated DRA with a 50%

bandwidth was successfully implemented. Additionally, [18] conducted an investigation on a probe-fed isosceles triangular DRA (TDRA), demonstrating an impedance bandwidth of 47.4%. However, these designs still faced challenges associated with high profiles.

In addition to the methods mentioned above, using higher-order modes of the DR can also expand the bandwidth of the DRAs [21], [22], [23], [24], [25], [26]. In [21], [22], [23], [24], the higher-order mode of the cylindrical DRA (HEM_{113} mode) [21], [23] or rectangular DRA (TE_{113}^{y} mode [22] or TE_{131} mode [24]) was utilized and can be moved in proximity to its fundamental mode by finely-tuning the geometric parameters of the DR, thus achieving an improved bandwidth by merging these two resonance modes. However, these designs have a limited increment in bandwidth as only one higher-order mode is utilized. In [25], [26], multiple higher-order modes such as $TM_{02\delta}$, $TM_{03\delta}$ and $TM_{04\delta}$ of the DRAs are amalgamated to enhance the bandwidth. However, the introduction of an annular column adds complexity to the antenna design. Additionally, this approach aims at enhancing bandwidth by leveraging the benefits of small-size DRAs and thin planar monopole antennas. As documented in [27], [28], [29], [30], hybrid antennas comprising ring DRAs excited by an axi-symmetric coaxial monopole were explored, resulting in an ultrawide bandwidth (UWB) response. Nevertheless, this method is constrained by a high profile with a height of $0.25\lambda_0$. In [31], a UWB DRA named inserted DRA excited by a coplanar waveguide with 5.08 mm thickness, approximately $0.1\lambda_0$, was exploited. Whereas, the antenna gain is below 3 dBi within the desired frequency band. Consequently, achieving a DRA with both a wide operating bandwidth and compactness simultaneously remains a challenging task.

In this paper, an effective design method is presented to widen the impedance bandwidth of the DRA by combining its fundamental $TM_{01\delta}$ mode, higher-order $TM_{021+\delta}$ mode and the probe mode. To reallocate the three radiating resonant modes in close proximity, a thin metal ring is inserted into the DR surrounding the feeding probe to perturb the E-field distribution of the higher-order mode. In this aspect, the resonant frequency of the $TM_{021+\delta}$ mode gradually decreases while the other two frequencies are maintained. Consequently, the three modes can be merged for bandwidth improvement. application of the perturbation technique [32], [33] to adjust the resonant frequency of the higher-order $TM_{021+\delta}$ mode for enhancing the bandwidth of the DRA. Compared to the aforementioned designs, the proposed configuration is much more compact and simple. With the benefits of wide bandwidth and a compact geometry, the proposed antenna emerges as a promising choice for vehicular applications.

The rest of this paper is organized as follows. In Section II, the basic principle of the DRA is investigated based on the *E*-field distributions and theoretical analysis. Section III presents the antenna geometry and measurement performances. Section IV provides a parametric study and corresponding discussion. Finally, Section V concludes the paper.

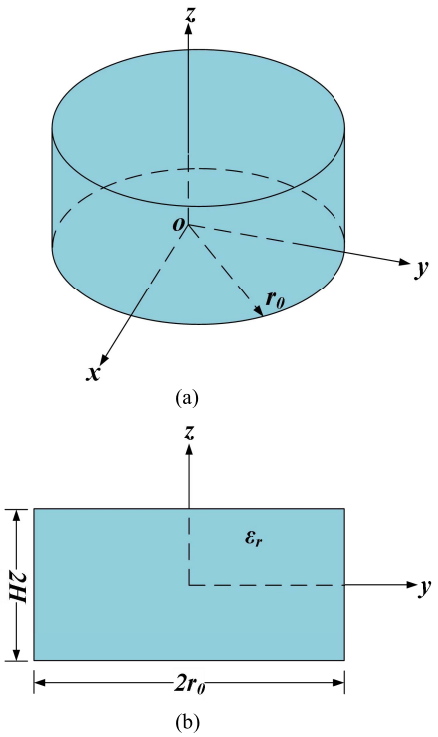

FIGURE 1. Geometry of the cylindrical DR with a permittivity of ε_r. (a) 3-D view; (b) front view.

II. THEORY

In this section, the basic principle of the proposed DRA is studied to illustrate how the resonant frequency of the higher-order mode of the antenna is decreased by loading the metal ring structure through the theoretical analysis.

A. E-FIELD DISTRIBUTIONS OF $TM_{01\delta}$ AND $TM_{02\delta}$ MODES

Considering a cylindrical DR as depicted in Fig. 1, it is with a permittivity of ε_r, a height of $2H$ and a radius of r_0, respectively. By using the eigenmode solver in *Ansys HFSS*, this DR is analyzed and the simulated *E*-field distributions of $TM_{01\delta}$ and $TM_{02\delta}$ modes are plotted in Fig. 2. It is observed that for $TM_{01\delta}$ mode, the *E*-field mainly focuses on the central of the DR with two nulls occurred at a distance of r away from the central of the DR. As for $TM_{02\delta}$ mode, the *E*-field intensities at the above two nulls are comparatively strong. It means that if a perturbation is introduced herein by using the metal structure, it would exert a serious influence on the E_z component of $TM_{02\delta}$ mode but only with a slight effect on that of $TM_{01\delta}$ mode. Thus, to facilitate it, the null areas of $TM_{01\delta}$ and $TM_{02\delta}$ modes are

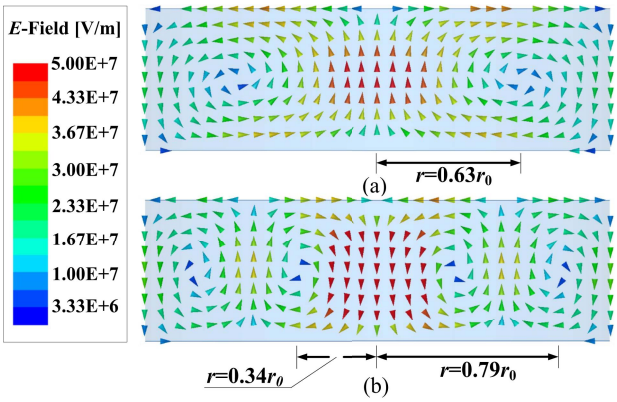

FIGURE 2. Simulated *E*-field distributions inside the DR. (a) $TM_{01\delta}$ mode; (b) $TM_{02\delta}$ mode.

primarily necessary to mathematically calculate for guiding the addition of the possible metal structure. The subsequent section provides a thorough presentation of the calculation processes for detailed analysis.

B. CALCULATION

According to [34], the E_z component of the $TM_{01\delta}$ or $TM_{02\delta}$ modes can be expressed as:

$$E_z = J_0(hr)cos(\beta z) \tag{1}$$

where J_0 is the zero-order *Bessel* function of the first kind. The values of h and β are the wavenumber in the r-direction and z-direction, respectively. The rough values of h and β can be determined by the assumption that the DR surfaces (including top, bottom and side surfaces) are considered as perfect magnetic walls. Then, h is enforced to satisfy the requirement [32]:

$$J_0'(hr_0) = 0 \tag{2}$$

For the case of the $TM_{01\delta}$ mode, h and β can be derived as

$$h = \frac{X_{01}'}{r_0} = \frac{3.832}{r_0} \tag{3}$$

$$\beta = \frac{\pi}{2H} \tag{4}$$

For the case of the $TM_{02\delta}$ mode, h_1 and β_1 can be derived as

$$h_1 = \frac{X_{02}'}{r_0} = \frac{7.016}{r_0} \tag{5}$$

$$\beta_1 = \frac{\pi}{2H} \tag{6}$$

where

$$J_0'(X_{0n}') = 0 \qquad (n = 1, 2, 3, \ldots) \tag{7}$$

Substituting (3) and (4) into (1), and let $E_z = 0$, it can be derived:

$$J_0\left(\frac{X_{01}'}{r_0}r\right) = 0 \tag{8}$$

Thereafter, the ratio of r and r_0 can be calculated by

$$\frac{X_{01}'}{r_0}r = X_{01} \tag{9}$$

$$\frac{r}{r_0} = \frac{X_{01}}{X_{01}'} = \frac{2.405}{3.832} = 0.63 \tag{10}$$

The results of the $TM_{02\delta}$ mode can be analyzed and derived in the similar way as follows:

$$J_0\left(\frac{X_{02}'}{r_0}r\right) = 0 \tag{11}$$

$$\frac{X_{02}'}{r_0}r = X_{0i}(i = 1, 2) \tag{12}$$

$$\frac{r}{r_0} = \frac{X_{01}}{X_{02}'} = \frac{2.405}{7.016} = 0.34 \tag{13}$$

$$\frac{r}{r_0} = \frac{X_{02}}{X_{02}'} = \frac{5.520}{7.016} = 0.79 \tag{14}$$

The calculation results show that at the radius of $r = 0.34r_0$ and $r = 0.79r_0$, the E_z component of the $TM_{02\delta}$ mode becomes zero. And as for the $TM_{01\delta}$ mode, the null point of the E_z component is occurred at $r = 0.63r_0$. Based on the analysis in Section II-A, it can be determined that the perturbation structure can work at the vicinity of $r = 0.63r_0$. The calculation results are also marked in Fig. 2.

It should be noted that the above calculations are also suitable for the $TM_{021+\delta}$ mode, because the value of h in the $TM_{02\delta}$ and $TM_{021+\delta}$ modes is the same under the perfect magnetic wall assumption. Therefore, the perturbation technique can be applied in the case of the $TM_{01\delta}$ and $TM_{021+\delta}$ modes which are employed in this design.

C. RELATIONSHIP BETWEEN E-FIELD AND RESONANT FREQUENCY

The preceding subsections focus on the examination and calculation of the radius suitable for introducing the perturbation technique, as determined through an analysis of the E-field distribution. The main objective of this paper is to devise a compact DRA with enhanced bandwidth by diminishing the resonant frequency of the $TM_{021+\delta}$ mode using the perturbation technique. To demonstrate the perturbation mechanism, the relationship between the *E*-field and the resonant frequency is investigated. For the $TM_{01\delta}$ mode of a cylindrical DR, the wavenumber k_0 in the air and the resonant frequency f_0 can be given by

$$\varepsilon_r k_0^2 = h^2 + \beta^2 \tag{15}$$

$$f_0 = \frac{k_0 c}{2\pi} \tag{16}$$

where c is the velocity of light in the free space. Once the values of h and β are known, f_0 can be calculated through (15) and (16). According to (1), h and β are used to describe the E_z component of the $TM_{01\delta}$ mode, and with reference to (15) and (16), the resonant frequency of the $TM_{01\delta}$ mode is also determined by h and β. It indicates that the perturbation of the *E*-field can be

reflected on the resonant frequency through h and β. Other modes of the DR can also be analyzed in a similar way. Therefore, the perturbation of the E-field will result in the variation of the resonant frequency.

Based on the above analysis, it can be concluded that at the radius of $r = 0.63r_0$, the perturbation can be introduced to alter the resonant frequency of the $TM_{021+\delta}$ mode. In this design, a thin metal ring serves as the perturbation structure. It is acknowledged that the metal surface can be treated as a perfect electric wall, and the E-field will be perpendicular to the perfect electric wall. Conversely, the E-field component parallel to the metal surface will minimize since the E-field distribution must adhere to the boundary condition. Hence, if a thin metal ring with a radius of $r = 0.63r_0$ is positioned axially within the DR, it can strongly influence the resonant frequency of the $TM_{021+\delta}$ mode by changing its E-field distribution. In contrast, the resonant frequency of the $TM_{01\delta}$ mode is only slightly affected because its E_z component at this location is the weakest. Most significantly, by judiciously introducing the metal structure, the volume of the DR can be significantly reduced [35], [36], [37]. Therefore, the metal ring serves not only as a perturbation structure to broaden the impedance bandwidth, but is also instrumental in creating a compact DRA geometry. These two advantages are of utmost significance for vehicular platform applications.

III. ANTENNA GEOMETRY AND MEASUREMENT

In order to validate the enhancement of bandwidth, this section compares the performance of DRA with and without the perturbation structure.

A. DRA WITHOUT PERTURBATION STRUCTURE

Fig. 3 shows the 3-D view of the DRA without the perturbation structure. It is a cylindrical DR with a permittivity of $\varepsilon_r = 16$, a height of $H_1 = 14$ mm and a radius of $a_1 = 23$ mm. A thin substrate ($\varepsilon_r = 2.2$) with a thickness of $h_s = 1$ mm is sandwiched between the ground and the DR. The ground plane is with a radius of $r_g = 46$ mm. The antenna is centrally fed by a coaxial probe to radiate the monopole-like pattern. To illustrate its frequency response, Fig. 4 shows the simulated $|S_{11}|$ of the structure. It can be seen from the figure that three resonant frequencies are generated in the frequency band of interest, but the impedance matching in the high-frequency band is worse, resulting in a narrow bandwidth. Fig. 5 displays the E-field distributions inside the DRA at 2.5 and 4.26 GHz, indicating that the first resonance is caused by the $TM_{01\delta}$ mode and the third one is due to the $TM_{021+\delta}$ mode. Also, it can be analyzed that the second mode is introduced by the feeding probe.

B. DRA WITH PERTURBATION STRUCTURE

To overcome the aforementioned impedance matching issue, a thin metal ring with a height of h_r and a thickness of t_1, acting as a perturbation structure, is added inside the DR as part of the proposed design, as depicted in Fig. 6.

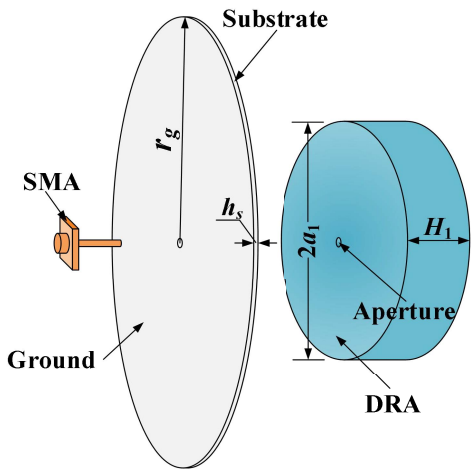

FIGURE 3. 3-D view of the DRA without the perturbation structure.

Based on the above investigation in Section II, the inner radius of the inserted metal ring is set as $r_1 = 0.63a_1$. In the following discussion, the sizes of the ground and the DR remain the same as those in Section III-A to facilitate a direct comparison. Fig. 8 depicts the simulated $|S_{11}|$ of the proposed antenna. Referring to the figure, it is observed that the third resonant frequency is notably shifted downward from 4.26 GHz to 3.94 GHz, whereas the resonant frequency of the $TM_{01\delta}$ mode slightly moves from 2.5 GHz to 2.58 GHz. To verify the operating modes of the DRA with inserted metallic ring, the E-field distributions of the DRA at 2.58 GHz and 3.94 GHz are given in Fig. 7. With reference to Fig. 5(a) and Fig. 7(a), the E-field distributions inside the DRA with and without inserted metallic ring are nearly the same when operating at the $TM_{01\delta}$ mode. As for the $TM_{021+\delta}$ mode, the DRA with and without the inserted metallic ring own similar E-field distributions, as shown in Fig. 5(b) and Fig. 7(b). This is as expected because, as discussed above, the inserted metal ring has a very slight perturbation effect on the $TM_{01\delta}$ mode due to the weak E-field intensity. Therefore, it can be concluded that the addition of the metal ring structure contributes to the bandwidth improvement. By merging the operating band of the $TM_{01\delta}$, $TM_{021+\delta}$ and probe modes together, a wide bandwidth is achieved. The -10 dB impedance bandwidth is significantly increased from 23.5% to 51.6% (2.39 GHz~4.05 GHz). Owing to the simple bandwidth-enhanced mechanism, the entire DRA configuration is very compact.

C. MEASUREMENT

For demonstration, a bandwidth-improved DRA was fabricated and tested. Photographs of the fabricated prototype are depicted in Fig. 8. Its geometrical parameters are listed in Table 1. In the prototype, the inserted metal ring inside the DR is realized through the metal plating process rather than by physically inserting a metal inside. Since the metal plating process is well-established, it does not introduce fabrication

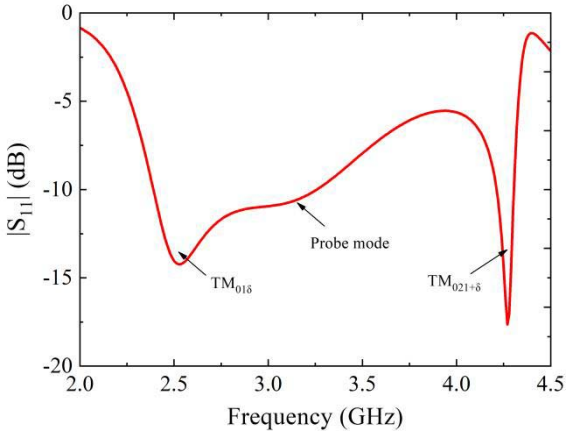

FIGURE 4. $|S_{11}|$ of the DRA without the perturbation structure.

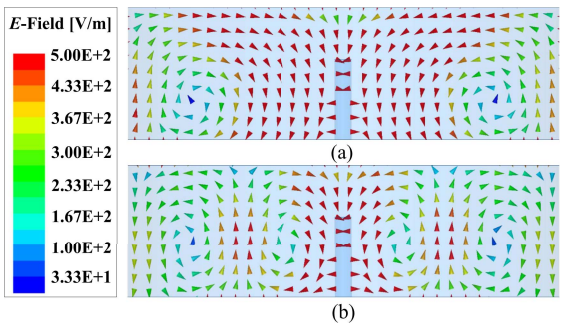

FIGURE 5. *E*-field distributions of the DRA without the perturbation structure. (a) 2.5 GHz; (b) 4.26 GHz.

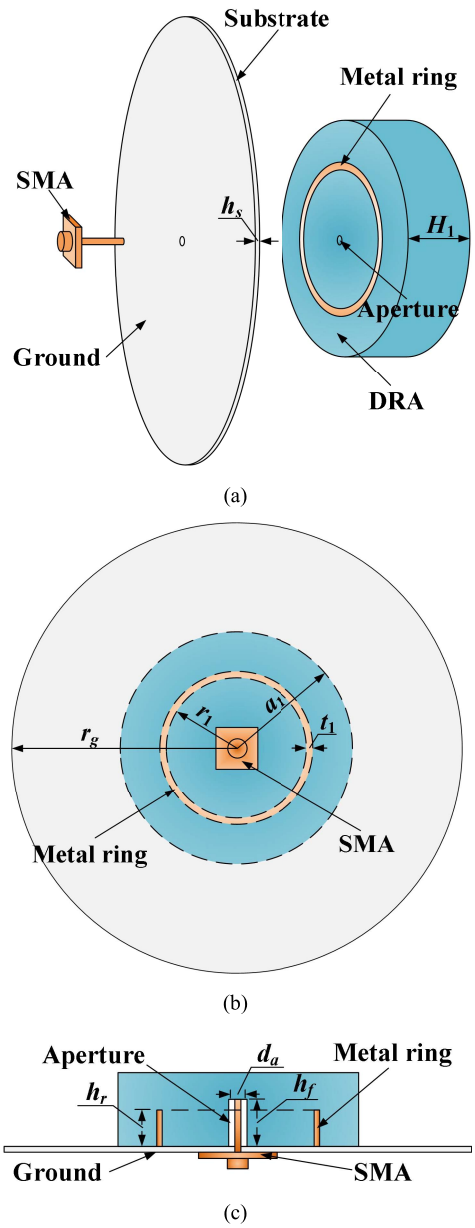

FIGURE 6. Geometry of the antenna with perturbation structure. (a) 3-D view; (b) Bottom view; (c) Cross section view.

complexity or high cost. The reflection coefficient was measured with a *Keysight N5225A* network analyzer, whereas the antenna gains and radiation patterns were obtained by using a near-field measurement system.

The measured $|S_{11}|$ of the prototype are presented in Fig. 9. It is observed that the measured operating band slightly shifts upward compared to the simulated one. The measured -10 dB impedance bandwidth is 51.1% (2.49 GHz~4.2 GHz), which is very close to the simulated one. The simulated and measured gains are also compared in Fig. 9. As can be seen from the figure, the measured in-band peak gain is given by 6.4 dBi, which corresponds well with the simulated result of 5.7 dBi. The simulated and measured efficiencies are compared in Fig. 10. As can be observed from the figure, the measured efficiency of the proposed DRA antenna is higher than 88% over the impedance pass-band. Good agreement is obtained between the simulated and measured results. The small deviation is mainly attributed to manufacturing, assembly and experimental tolerance.

The simulated and measured radiation patterns of the prototype in the elevation (*xoz*-plane) and azimuth (*xoy*-plane) planes at 2.6 GHz and 3.9 GHz are plotted in Fig. 11. In the elevation plane, there is a radiation null in the boresight direction ($\theta = 0^{o}$), while the azimuth radiation pattern is omnidirectional. Moreover, the elevation angle corresponding to the maximum radiation decreases as the frequency increases. This is reasonable because the electrical size of the ground plane increases with frequency. Radiation patterns at other frequencies are also measured and they remain stable across the passband.

IV. PARAMETRIC STUDY AND DISCUSSION

A parametric study is carried out to further demonstrate the working mechanism of the design. The simulated $|S_{11}|$ with different values of h_r is depicted in Fig. 12. It is observed that the resonant frequency of the $TM_{021+\delta}$ mode gradually decreases as the value of h_r increases, and the resonant

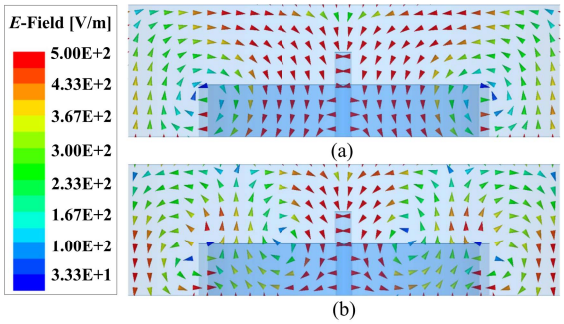

FIGURE 7. *E*-field distributions of the DRA with the perturbation structure. (a) 2.58 GHz; (b) 3.94 GHz.

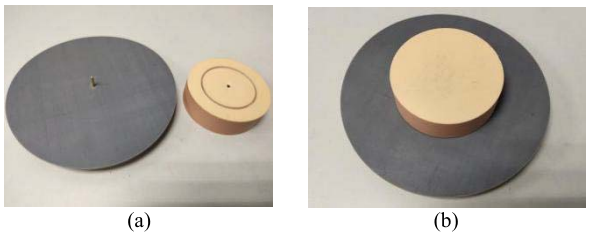

FIGURE 8. Photographs of the prototype: (a) Disassembly view; (b) Assembly view.

TABLE 1. Dimensions of the proposed antenna.

Parameters	a_1	H_1	r_g	r_1	t_1
Values/mm	23	14	46	14.5	1
Parameters	h_r	d_a	h_f	h_s	
Values/mm	5.5	1.8	9	1	

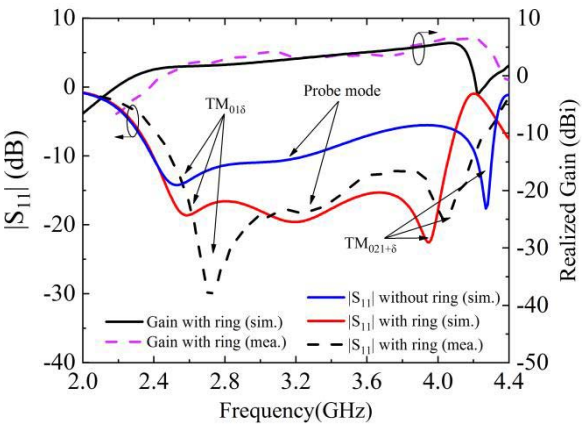

FIGURE 9. Simulated and measured results of the proposed antenna.

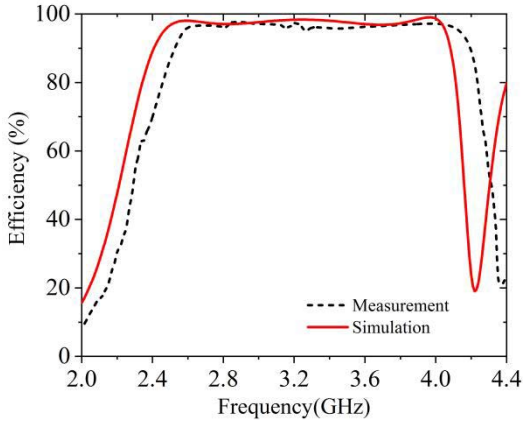

FIGURE 10. Simulated and measured efficiency of the proposed antenna.

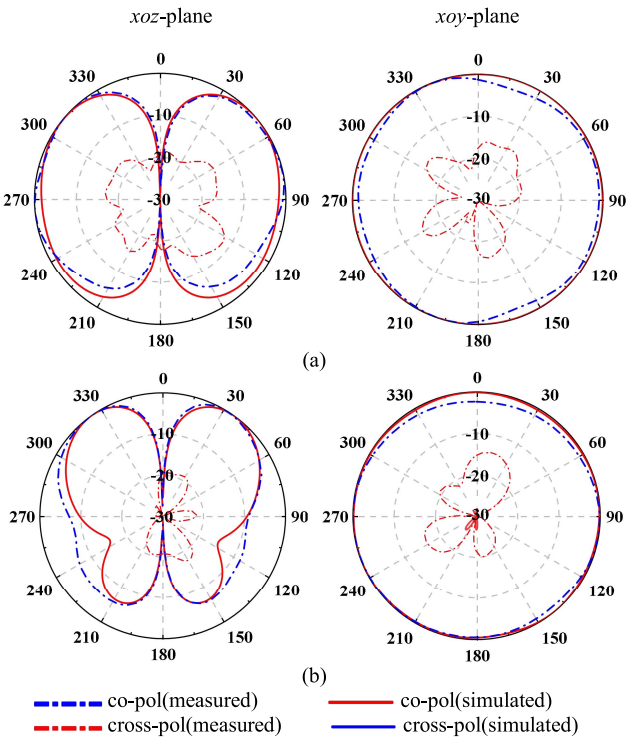

FIGURE 11. Simulated and measured radiation patterns of the antenna. (a) 2.6 GHz; (b) 3.9 GHz.

frequency of the $TM_{01\delta}$ mode moves slightly. It is reasonable because as the value of h_r increases, h and β of the $TM_{021+\delta}$ mode vary significantly, resulting in a large fluctuation in the resonant frequency. On the other hand, the values of h and β in $TM_{01\delta}$ mode are affected slightly, maintaining a relatively stable resonant frequency.

The comparison of the proposed design with some previously reported works in terms of the footprint, profile, impedance bandwidth, etc. is summarized in Table 2. It can be seen that the designs in [9], [18], and [20] use stacked DR, triangular DR and high aspect ratio DR structures for impedance-bandwidth improvement. However, this method has an effect on antennas' profile, hence are not suitable for low-profile platform applications. A conical-shaped DRA in [17] is developed to reduce the antenna height to $0.17\lambda_0$. In [15], [16], the DRA mode and the shorting-pin mode [15] or aperture mode [16] are skillfully combined to enhance the bandwidth with a height of $\sim 0.1\lambda_0$. In [24], a lower-profile DRA ($0.07\lambda_0$) with extended bandwidth by properly modifying the dielectric characteristics of the designated region is presented. However, the obtained impedance bandwidths of these designs are not wide enough. A broad bandwidth of more than 90% is realized by combining a

TABLE 2. Comparison of the proposed and reported antennas.

Reference	Method of bandwidth enhancement	Permittivity of DR	Footprint/λ_0^2	Profile/λ_0	Mode	BW (GHz)	BW (%)
[9]	Staked double annular ring	ε_{r1}=36, ε_{r2}=4	0.34*0.34	0.24	End-fire mode	3.6-5.5	42%
[15]	Perturbation structure	ε_r=16	0.32*0.32	0.09	TM_{011}, shorting-pin mode	3.65-4.33	17%
[16]	Apertures-fed technique	ε_r=6.85	2.55*2.55	0.11	TM_{011}, $TM_{02\delta}$, aperture mode	4.88–6.88	34%
[17]	Modified DR (Conical)	ε_r=9.8	0.62*0.62	0.17	$TM_{01\delta}$	3.4-5	38.1%
[18]	Modified DR (Tri-angular)	ε_r=10	0.36*0.19	0.36	TM^Z_{101}, TM^Z_{103}	4.33-7.02	47.4%
[20]	Modified DR (High aspect ratio)	ε_r=6.85	0.29*0.29	0.39	TE_{111}^y, TE_{113}^y	2.99-4.8	46%
[24]	Modified dielectric characteristics	ε_{r1}=45, ε_{r2}=69	0.35*0.35	0.07	TE_{111}, TE_{131}	9.12-10.84	17.3%
[25]	Multi-ring structure	ε_{r1}=10, ε_{r2}=8.25, ε_{r3}=4, ε_{r4}=2.5	1.54*1.54	0.19	$TM_{01\delta}$, $TM_{02\delta}$, $TM_{03\delta}$	4.3-8	60.2%
[26]	Annular column loaded structure	ε_{r1}=9.8, ε_{r2}=16	1.04*1.04	0.18	$TM_{01\delta}$, $TM_{02\delta}$, $TM_{03\delta}$, $TM_{04\delta}$	3.14-5.56	56%
[28]	Combination of monopole and DRA	ε_r=10	0.28*0.28	0.43	$TM_{01\delta}$, monopole mode	4.5-12.5	94.1%
This work	Perturbation structure	ε_r=16	0.51*0.51	0.16	$TM_{01\delta}$, $TM_{021+\delta}$	2.49-4.2	51.1%

BW represents bandwidth

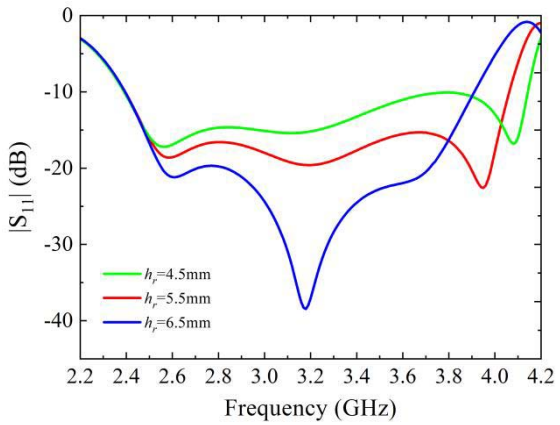

FIGURE 12. Simulated $|S_{11}|$ of the antenna with different values of h_r.

monopole antenna and a DRA, but its profile is as high as $0.43\lambda_0$ [28]. The designs presented in [25] and [26] have similar antenna profiles and impedance bandwidths as the proposed one, nevertheless, these designs have the disadvantages of bulky volume or a large footprint. In contrast to many previously reported designs, the proposed work not only has a simple and compact antenna structure, but also possesses a bandwidth of more than 50%. Moreover, the structure is simple and easy to be fabricated. Hence, the results indicate that the proposed design is a promising candidate for vehicular platform applications.

V. CONCLUSION

A compact DRA with improved bandwidth has been investigated in this paper. A thin metal ring was employed as a perturbation structure to reduce the resonant frequency of $TM_{021+\delta}$ mode of DRA. It has been shown that the fundamental $TM_{01\delta}$ mode, the higher-order $TM_{021+\delta}$ mode and probe mode can be simultaneously excited to achieve a wide bandwidth with conical radiation patterns. The proposed bandwidth-improved methodology results in a simple and compact antenna configuration. A prototype was fabricated and measured to validate the design. Simulation and measurement results showed good agreement, revealing that the −10 dB impedance bandwidth could be increased from 23.5% to 51.6% using the proposed perturbation structure. With advantages such as wide bandwidth, well-controlled radiation patterns, compact size, and ease of fabrication, the proposed design holds promising prospects for applications in vehicular communication systems.

REFERENCES

[1] S. Long, M. McAllister, and L. Shen, "The resonant cylindrical dielectric cavity antenna," *IEEE Trans. Antennas Propag.*, vol. 31, no. 3, pp. 406–412, May 1983.
[2] K. W. Leung, E. H. Lim, and X. S. Fang, "Dielectric resonator antennas: From the basic to the aesthetic," *Proc. IEEE*, vol. 100, no. 7, pp. 2181–2193, Jul. 2012.
[3] B. Mukherjee, P. Patel, and J. Mukherjee, "A review of the recent advances in dielectric resonator antennas," *J. Electrom. Waves Appl.*, vol. 34, no. 9, pp. 1095–1158, Apr. 2020.
[4] B. Mukherjee and M. Chauhan, *Dielectric Resonator Antennas: From Design to Recent Trends*. London, U.K.: Artech House, 2022.
[5] H. Wong, K. K. So, and X. Gao, "Bandwidth enhancement of a monopolar patch antenna with V-shaped slot for car-to-car and WLAN communications," *IEEE Trans. Veh. Technol.*, vol. 65, no. 3, pp. 1130–1136, Mar. 2016.
[6] M. G. N. Alsath et al., "An integrated tri-band/UWB polarization diversity antenna for vehicular networks," *IEEE Trans. Veh. Technol.*, vol. 67, no. 7, pp. 5613–5620, Jul. 2018.
[7] I. K. Kim, H. Wang, S. J. Weiss, and V. V. Varadan, "Embedded wideband metaresonator antenna on a high-impedance ground plane for vehicular applications," *IEEE Trans. Veh. Technol.*, vol. 61, no. 4, pp. 1665–1672, May 2012.
[8] A. A. Kishk, X. Zhang, A. W. Glisson, and D. Kajfez, "Numerical analysis of stacked dielectric resonator antennas excited by a coaxial probe for wideband applications," *IEEE Trans. Antennas Propag.*, vol. 51, no. 8, pp. 1996–2006, Aug. 2003.

[9] Y.-X. Guo, Y.-F. Ruan, and X.-Q. Shi, "Wide-band stacked double annular-ring dielectric resonator antenna at the end-fire mode operation," *IEEE Trans. Antennas Propag.*, vol. 53, no. 10, pp. 3394–3397, Oct. 2005.
[10] A. G. Walsh, C. S. De Young, and S. A. Long, "An investigation of stacked and embedded cylindrical dielectric resonator antennas," *IEEE Antennas Wireless Propag. Lett.*, vol. 5, pp. 130–133, 2006.
[11] Q. Rao, T. A. Denidni, and A. R. Sebak, "Broadband compact stacked T-shaped DRA with equilateral-triangle cross sections," *IEEE Microw. Wireless Compon. Lett.*, vol. 16, no. 1, pp. 7–9, Jan. 2006.
[12] W. Huang and A. A. Kishk, "Compact wideband multi-layer cylindrical dielectric resonator antennas," *IET Microw. Antennas Propag.*, vol. 1, no. 5, pp. 998–1005, Oct. 2007.
[13] Y.-M. Pan and K. W. Leung, "Wideband circularly polarized dielectric bird-nest antenna with conical radiation pattern," *IEEE Trans. Antennas Propag.*, vol. 61, no. 2, pp. 563–570, Feb. 2013.
[14] Y. M. Pan and S. Y. Zheng, "A low-profile stacked dielectric resonator antenna with high-gain and wide bandwidth," *IEEE Antennas Wireless Propag. Lett.*, vol. 15, pp. 68–71, 2016.
[15] N.-W. Liu, X.-P. Chen, L. Zhu, Z.-X. Liu, and G. Fu, "Compact dielectric resonator antenna with bandwidth enhancement via loading of shorting pins," *IET Microw. Antennas Propag.*, vol. 13, no. 12, pp. 1969–1973, 2019.
[16] X. S. Fang, L. P. Weng, and Z. Fan, "Design of the wideband and low-height omnidirectional cylindrical dielectric resonator antenna using arced-apertures feeding," *IEEE Access*, vol. 11, pp. 20128–20135, 2023.
[17] G. Almpanis, C. Fumeaux, J. Fröhlich, and R. Vahldieck, "A truncated conical dielectric resonator antenna for body-area network applications," *IEEE Antennas Wireless Propag. Lett.*, vol. 8, pp. 279–282, 2009.
[18] S. Maity and B. Gupta, "Experimental investigations on wideband triangular dielectric resonator antenna," *IEEE Trans. Antennas Propag.*, vol. 64, no. 12, pp. 5483–5486, Dec. 2016.
[19] R. Chair, A. A. Kishk, K. F. Lee, and C. E. Smith, "Wideband flipped staired pyramid dielectric resonator antennas," *Electron. Lett.*, vol. 40, no. 10, pp. 581–582, May 2004.
[20] X. S. Fang, K. P. Shi, and Y. X. Sun, "Design of the single-/dual-port wideband differential dielectric resonator antenna using higher order mode," *IEEE Antennas Wireless Propag. Lett.*, vol. 19, pp. 1605–1609, 2020.
[21] Y. X. Sun and K. W. Leung, "Dual-band and wideband dual-polarized cylindrical dielectric resonator antennas," *IEEE Antennas Wireless Propag. Lett.*, vol. 12, pp. 384–387, 2013.
[22] X. S. Fang and K. W. Leung, "Designs of single- dual- wideband rectangular dielectric resonator antennas," *IEEE Trans. Antennas Propag.*, vol. 59, no. 6, pp. 2409–2414, Jun. 2011.
[23] X. S. Fang and K. W. Leung, "Linear-/circular-polarization designs of dual-/wide-band cylindrical dielectric resonator antennas," *IEEE Trans. Antennas Propag.*, vol. 60, no. 6, pp. 2662–2671, Jun. 2012.
[24] J.-E. Zhang, Q. Zhang, W. Kong, W.-W. Yang, and J.-X. Chen, "Compact and low-profile linear-/circular-polarization dielectric resonator antennas with extended bandwidths," *IEEE Open J. Antennas Propag.*, vol. 3, pp. 391–397, 2022.
[25] Z.-X. Xia, K. W. Leung, and K. Lu, "3-D-printed wideband multi-ring dielectric resonator antenna," *IEEE Antennas Wireless Propag. Lett.*, vol. 18, pp. 2110–2114, 2019.
[26] Y. He, Y. Lin, C. Deng, and Z. Feng, "Annular column loaded cylindrical dielectric resonator antenna for wideband conical radiation," *IEEE Trans. Antennas Propag.*, vol. 63, no. 12, pp. 5874–5878, Dec. 2015.
[27] M. Lapierre, Y. M. M. Antar, A. Ittipiboon, and A. Petosa, "Ultra wideband monopole/dielectric resonator antenna," *IEEE Microw. Wireless Compon. Lett.*, vol. 15, no. 1, pp. 7–9, Jan. 2005.
[28] D. Guha, Y. M. M. Antar, A. Ittipiboon, A. Petosa, and D. Lee, "Improved design guidelines for the ultra wideband monopole-dielectric resonator antenna," *IEEE Antennas Wireless Propag. Lett.*, vol. 5, pp. 373–376, 2006.
[29] D. Guha, B. Gupta, and Y. M. M. Antar, "Hybrid monopole-DRAs using hemispherical/conical-shaped dielectric ring resonators: Improved ultra-wideband designs," *IEEE Trans. Antennas Propag.*, vol. 60, no. 1, pp. 393–398, Jan. 2012.
[30] C. Ozzaim, "Monopole antenna loaded by stacked annular ring dielectric resonators for ultrawide bandwidth," *Microw. Opt. Technol. Lett.*, vol. 56, no. 10, pp. 2395–2398, 2014.
[31] K. S. Ryu and A. A. Kishk, "UWB dielectric resonator antenna having consistent omnidirectional pattern and low cross-polarization characteristics," *IEEE Trans. Antennas Propag.*, vol. 59, no. 4, pp. 1403–1408, Apr. 2011.
[32] D. Guha, H. Gajera, and C. Kumar, "Cross-polarized radiation in a cylindrical dielectric resonator antenna: Identification of source experimental proof and its suppression," *IEEE Trans. Antennas Propag.*, vol. 63, no. 4, pp. 1863–1867, Apr. 2015.
[33] D. Guha, H. Gajera, and C. Kumar, "Perturbation technique to improve purity of modal fields in dielectric resonator antenna resulting in reduced cross-polarized radiation," *IEEE Trans. Antennas Propag.*, vol. 63, no. 7, pp. 3253–3257, Jul. 2015.
[34] R. K. Mongia and P. Bhartia, "Dielectric resonator antennas-a review and general design relations for resonant frequency and bandwidth," *Int. J. Microw. Millim.-Wave Comput.-Aided Eng.*, vol. 4, pp. 230–247, Jul. 1994.
[35] M. T. K. Tam and R. D. Murch, "Half volume dielectric resonator antenna designs," *Electron. Lett.*, vol. 33, no. 23, pp. 1914–1916, 1997.
[36] S. Gotra, G. Varshney, R. S. Yaduvanshi, and V. S. Pandey, "Dual-band circular polarisation generation technique with the miniaturisation of a rectangular dielectric resonator antenna," *IET Microw. Antennas Propag.*, vol. 13, no. 10, pp. 1742–1748, 2019.
[37] S. G. O'Keefe, S. P. Kingsley, and S. Saario, "FDTD simulation of radiation characteristics of half-volume HEM- and TE-mode dielectric resonator antennas," *IEEE Trans. Antennas Propag.*, vol. 50, no. 2, pp. 175–179, Feb. 2002.

HUI GU was born in Jiangsu, China. He received the B.S. degree in electronics and information engineering from Huaiyin Normal University, China, in 2012, the M.S. degree in communication and information system from the Nanjing University of Science and Technology, Nanjing, China, in 2016, and the Ph.D. degree in information and communication engineering from Shenzhen University, Shenzhen, China, in 2021.

He is currently an Assistant Professor with the School of Electronics and Information, Hangzhou Dianzi University, Hangzhou, China. His recent research interest focuses on wideband antennas, reconfigurable circuits and antennas, and antenna in package.

LEI GE (Senior Member, IEEE) was born in Jiangsu, China. He received the B.S. degree in electronic engineering from the Nanjing University of Science and Technology, Nanjing, China, in 2009, and the Ph.D. degree in electronic engineering from the City University of Hong Kong, Hong Kong, in 2015.

From September 2010 to July 2011, he was a Research Assistant with the City University of Hong Kong, where he was a Postdoctoral Research Fellow with the State Key Laboratory of Millimeter Waves from April 2015 to October 2015. He is currently an Associate Professor with the State Key Laboratory of Radio Frequency Heterogeneous Integration, Shenzhen University, China. His recent research interest focuses on multifunction integrated antennas, reconfigurable antennas, and wideband and multiband antennas.

Dr. Ge received the Honorable Mention at the Student Contest of the 2012 IEEE APS-URSI Conference and Exhibition held in Chicago, USA, and the first Prize in the Student Innovation Competition of the 2014 IEEE International Workshop on Electromagnetics held in Sapporo, Japan, in 2014. He was a recipient of the IEEE Antennas and Propagation Society Outstanding reviewer Award from 2017 to 2018. He was the TPC co-chair, a TPC member, a workshop/tutorial chair, and the session chair of some international conferences.